

Intrinsic statistical regularity of topological charges revealed in dynamical disk model

Ranzhi Sun and Zhenwei Yao*

*School of Physics and Astronomy, and Institute of Natural Sciences,
Shanghai Jiao Tong University, Shanghai 200240, China*

Identifying ordered structures hidden in the packings of particles is a common scientific question in multiple fields. In this work, we investigate the dynamical organizations of a large number of initially randomly packed repulsive particles confined on a disk under the Hamiltonian dynamics by the recently developed algorithm called the random batch method. This algorithm is specifically designed for reducing the computational complexity of long-range interacting particle systems. We highlight the revealed intrinsic statistical regularity of topological charges that is otherwise unattainable by the continuum analysis of particle density. We also identify distinct collective dynamics of the interacting particles under short- and long-range repulsive forces. This work shows the robustness and effectiveness of the concept of topological charge for characterizing the convoluted particle dynamics, and demonstrates the promising potential of the random batch method for exploring fundamental scientific questions arising in a variety of long-range interacting particle systems in soft matter physics and other relevant fields.

I. INTRODUCTION

The packing of interacting particles in confined geometries is a common theme in a host of soft matter systems [1–7]. In particular, the confluence of theoretical and experimental investigations in the past few decades on the static two-dimensional(2D) packing problem on both flat [8–14] and curved [15–18] spaces reveals the crucial role of topological defects in the organizations of the particles. Disclinations as a kind of fundamental topological defect emerge in the crystalline packings of particles on curved spaces [15–17] or under mechanical [9, 19, 20] and thermal [21, 22] stimuli. In a triangular lattice, a p -fold disclination refers to a vertex of coordination number p , and it carries topological charge $6 - p$ [15, 17]. According to the continuum elasticity theory, in analogy to electric charges, disclinations of the same sign repel and unlike signs attract [15]. These particle-like excitations are actively involved in several important physical processes, such as the screening of the substrate curvature [16, 23, 24] and the healing of the disrupted crystalline order [25–27].

In our previous work on the inhomogeneous static packings of particles in mechanical equilibrium confined on a disk, the unique perspective of a topological defect allows us to reveal the characteristically negative sign of the total topological charge Q and the associated hyperbolic geometry [10]. Recently, the static disk model was extended to the dynamical regime [28]. It was found that in the statistical sense, the hyperbolic geometry as reflected by the negative sign of the time-averaged total topological charge $\langle Q \rangle$ is preserved in the convoluted dynamical evolution of the particle configuration [28].

However, in our previous work the dynamical disk model consisted of a relatively small number of particles as limited by the long computational time [28]. It is

thus still not clear if the revealed statistical regularity of topological charges is caused by the boundary effect or due to the intrinsic effect of the long-range force. Elucidating this issue yields insights into the intrinsic order in seemingly irregular and temporally-varying packings of particles arising in the physical systems of charged colloids [17], complex (dusty) plasmas [29, 30], and a variety of charged entities at the nanoscale in electrolyte environments [31]. Furthermore, the relatively small number of particles in the previously studied disk model hinders one from performing a coarse-graining procedure to reveal and analyze the underlying flow patterns created by the repulsive forces of varying range.

To address these questions, it is crucial to extend the dynamic disk model to the large- N regime, where N is the number of particles. The challenge for simulating the dynamics of a long-range interacting system comes from the high computational complexity: the computation time is on the order of $O(N^2)$ per time step, and the whole simulation process involves up to one million simulation steps. To solve this problem, we employ the recently developed algorithm called the random batch method (RBM), which is specifically designed for reducing the computational complexity of long-range interacting particle systems down to the order of $O(N)$ [32, 33]. Numerical experiments show that the RBM is capable of capturing both transient dynamical structures [34] and crucial statistical features [35].

The goal of this work is to employ the powerful computational tool of the RBM for exploring the statistical and dynamical physics of the disk model consisting of a large number of repulsive particles (up to 150,000). Specifically, we aim at identifying the intrinsic statistical regularity of topological charges, and studying the flow patterns under the repulsive forces of varying range. To this end, in our model the particles confined on the disk interact by the screened Coulomb potential; the range of the force is conveniently controlled by the screening length. In the initial state, both the positions and the velocities of the particles are randomly distributed. The

*zyao@sjtu.edu.cn

motion of the particles under the interacting force is governed by the deterministic Hamiltonian dynamics. The equations of motion are numerically integrated by the standard Verlet method [36].

The main results of this work are presented below. By analyzing the trajectories of 150,000 particles, we show that under a long-range repulsive force, the time-averaged total topological charge $\langle Q \rangle$ is intrinsically negative corresponding to the hyperbolic geometry. Systematic simulations of the disk model at varying screening length show the regulation of the defect structure by the range of the repulsive force. These results suggest the robustness and effectiveness of the concept of topological charge for characterizing the convoluted particle dynamics at varying interaction range. Furthermore, we reveal the distinct dynamical organizations of the particles under short- and long-range repulsive forces by analyzing the coarse-grained velocity fields, and we demonstrate the capability of the RBM in capturing featured dynamical structures such as vortices and radial flows. In this work, the revealed intrinsic statistical regularity of topological charges and the featured flow patterns advance our understanding on the convoluted dynamical organizations of geometrically confined repulsive particles.

II. MODEL AND METHOD

The model consists of N identical point particles of mass m confined on a disk of radius r_0 ; the particles interact by the pairwise screened Coulomb potential. The evolution of the particle configuration is governed by the deterministic Hamiltonian dynamics (without introducing any thermal noise):

$$H = \sum_{i=1}^N \frac{p_i^2}{2m} + \sum_{i \neq j} \frac{\beta}{r_{ij}} \exp\left(-\frac{r_{ij}}{\lambda}\right) \quad (1)$$

where \vec{p}_i is the momentum of particle i , r_{ij} is the distance between particles i and j , λ is the screening length, and $\beta = q_0^2/(4\pi\epsilon)$, where ϵ is the dielectric constant. The rigid boundary condition is implemented by the reflection of particle trajectory at the boundary. In this work, the units of mass, length and time are the particle mass m , the mean distance of nearest particles a , and τ_0 . $\tau_0 = \sqrt{ma^3/\beta}$. The units of velocity and force are thus a/τ_0 and β/a^2 . Under the assumption that the particles are arranged in a triangular lattice, the lattice spacing a is estimated as

$$\frac{a}{r_0} = \sqrt{\frac{2\pi}{\sqrt{3}N}}. \quad (2)$$

In the initial state, the velocity \vec{v}_{ini} of each particle is random in both magnitude and direction; $v_{\text{ini}} \in (0, 1)$ and $\theta \in (0, 2\pi)$, where θ is the angle of the velocity vector \vec{v}_{ini} with respect to some reference direction. The initial positions of the particles are randomly distributed by the

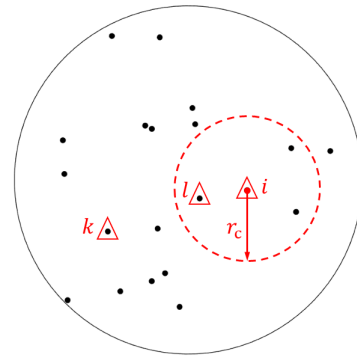


FIG. 1: Schematic plot for illustrating the random batch method. The particles on the disk are represented by the black dots. The particles marked by small triangles belong to the same batch Ω_p . The adjacent particles surrounding the particle concerned (labeled i) are located in the dashed circle of radius r_c .

procedure of random disk packing. The technical details are presented in Appendix A. We employ the standard Verlet method to numerically integrate the equations of motion under the specified rigid boundary condition and the random initial conditions [36]. Specifically, the position of particle i at time $t + 2h$ is determined by its positions at times $t + h$ and t via

$$\vec{x}_i(t + 2h) = 2\vec{x}_i(t + h) - \vec{x}_i(t) + \ddot{\vec{x}}_i(t + h)h^2 + \mathcal{O}(h^4),$$

where the step size $h = 10^{-3}$ in simulations. The most time-consuming procedure in the Verlet integration scheme for the long-range interacting particle system is the calculation of the forces. The computation time is on the order of $O(N^2)$ per time step. This imposes a challenge to explore the large- N systems of interest.

To resolve this issue, we employ the recently developed algorithm named the random batch method (RBM) by mathematicians [32, 33, 37]. This algorithm is specifically designed for reducing the computing time for long-range interacting particle systems down to the order of $O(N)$. In the following, we introduce our method of calculating force using RBM. Consider a system consisting of a large number of point particles with pairwise interaction. First, the interacting force on particle i by particle j , \vec{f}_{ij} , is decomposed into two parts [33]:

$$\begin{aligned} \vec{f}_{ij}(r_{ij}) &= \vec{f}_{ij}(r_{ij})[1 - H(r_{ij} - r_c)] \\ &\quad + \vec{f}_{ij}(r_{ij})H(r_{ij} - r_c) \\ &\equiv \vec{f}_{ij}^{(1)} + \vec{f}_{ij}^{(2)} \end{aligned} \quad (3)$$

where the Heaviside step function

$$H(r_{ij} - r_c) = \begin{cases} 1 & r_{ij} \geq r_c \\ 0 & r_{ij} < r_c. \end{cases}$$

r_{ij} is the distance between particle i and particle j . r_c is some cutoff distance that is comparable with the mean distance of nearest particles (see Fig. 1). Now, the total force on particle i can be written as

$$\vec{F}_i = \sum_{j \neq i} \vec{f}_{ij}^{(1)} + \sum_{j \neq i} \vec{f}_{ij}^{(2)}, \quad (4)$$

The first term in Eq. (4) is the sum of the forces exerted by all of the adjacent particles of particle i within the circular region of radius r_c , which is calculated rigorously. The second term involves the forces from all of the remaining particles, and it is approximated by the RBM to promote computational efficiency.

The schematic plot for illustrating the RBM is presented in Fig. 1. All of the N particles on the disk are labeled from 1 to N . For each instantaneous particle configuration in the time evolution, the N particles are randomly divided into a certain number of small batches by the particle labels (not by the particle positions). Each batch contains p particles. In Fig. 1, the particles marked by small triangles belong to the same batch Ω_p ; $p = 3$ in this case. Only the particles belonging to the same batch as particle i are counted in the calculation for the second term in Eq. (4). The summation of the forces from these particles is denoted as \vec{F}_{batch} . Multiplying \vec{F}_{batch} by a factor of $(N-1)/(p-1)$ gives the approximate value for the second term in Eq. (4). To conclude, the total force on particle i is approximated by [33]

$$\vec{F}_i = \sum_{r_{ij} < r_c} \vec{f}_{ij} + \frac{N-1}{p-1} \sum_{j \in \Omega_p} \vec{f}_{ij}(\vec{x}_{ij}) H(|\vec{x}_{ij}| - r_c). \quad (5)$$

In this work, the value of p is taken to be 2 by following the convention [37]. Note that due to the random selection of the particles, the RBM brings in random forces on the particles, which results in a monotonous increase of the kinetic energy (temperature). For the sake of the conservation of total energy, we perform the procedure of cooling in simulations (see Appendix B). Specifically, the velocity of each particle is rescaled by a common factor once the amount of the increased energy exceeds some threshold value, which is set to be about 5% of the total energy in the initial state.

Numerical experiments show that the RBM is capable of capturing both transient dynamical structures [34] and crucial statistical features [35]. The RBM works well in a series of statistical and dynamical problems, such as the Dyson Brownian motion, Thomson's problem, stochastic dynamics of wealth and opinion dynamics [37]. This algorithm has wide applications in quantum physics [32, 38, 39], plasma physics [40], hydromechanics [35], machine learning [41], chemistry and materials [34]. In this work, the RBM is used as a powerful tool for exploring the physics of long-range interacting systems containing a large number of particles (up to 150,000).

III. RESULTS AND DISCUSSION

In this section, we discuss the dynamics of the particles on the disk under both short- and long-range repulsive forces. In Sec. III A, the particle configurations are analyzed from the perspective of the underlying topological defect structure. Statistical regularity in the distribution of topological charge is revealed. In Sec. III B, we analyze the characteristic coarse-grained velocity field, and we reveal the distinct flow patterns created by the short- and long-range repulsive forces. We also discuss the relaxation of particle speed in both short- and long-range interacting systems.

A. Statistical regularity in the distribution of topological charge

We first briefly introduce the concept of a topological defect in a triangular lattice [15, 42]. By the standard Delaunay triangulation, the neighbors of each particle on the plane are uniquely determined, and the topological charge q_i for any particle i is defined by the formula

$$q_i = 6 - z_i, \quad (6)$$

where z_i is the coordination number of particle i [15]. A particle of coordination number z is called a z -fold disclination. In analogy to electric charges, disclinations of the same sign repel and unlike signs attract according to the continuum elasticity theory [15]. Topological defect is an important entity and a useful concept for understanding a series of elastic and plastic behaviors of crystals [7, 10, 16, 17].

In previous work, we analyzed the static equilibrium distribution of the long-range repulsive particles on the disk from the unique perspective of topological defects [10]. Specifically, we focused on the total topological charge Q :

$$Q \equiv \sum_{r_i < r'} q_i, \quad (7)$$

where r_i is the distance of the particle i carrying topological charge q_i to the center of the disk. The sum is over all of the topological charges within the circular domain of radius r' . r' is smaller than the radius of the disk by one lattice spacing. It is found that due to the intrinsic inhomogeneity created by the long-range electrostatic force, the sign of the total topological charge is negative, implying the existence of a hyperbolic geometric structure underlying the inhomogeneity phenomenon of particle packings [10].

The static disk model was recently extended to the dynamical regime, and the temporally-varying particle configurations on the disk were analyzed in terms of topological defects [28]. An important observation is that the time-averaged total topological charge $\langle Q \rangle$ is still negative in the dynamical regime; the value of $\langle Q \rangle$ is obtained

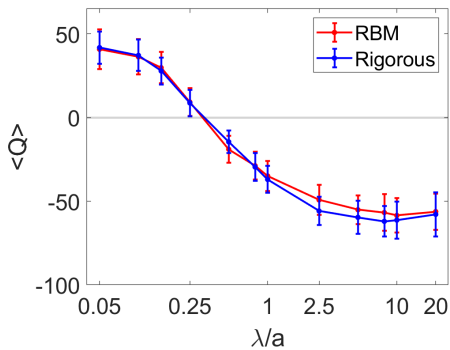


FIG. 2: Statistical regularity revealed from the perspective of total topological charge Q in the relatively small system of $N = 5000$. The $\langle Q \rangle$ - λ curves in red and blue show the results obtained by the RBM and the rigorous calculations, respectively. The statistical analysis of the total topological charge Q is based on 100 particle configurations of equal time interval $0.5\tau_0$ during $t \in [50.5\tau_0, 100\tau_0]$. The error bars indicate the magnitude of the standard deviations of Q . The initial conditions for both cases are identical.

by averaging over 100 statistically independent instantaneous particle configurations after the system reaches equilibrium. In other words, in the statistical sense, the characteristically negative sign of the total topological charge as found in the static disk model is preserved in the complicated dynamical evolution of the particle configuration. Furthermore, it is found that the sign of the time-averaged total topological charge $\langle Q \rangle$ switches from positive to negative with the increase in the range of interaction.

However, the revealed statistical regularity in $\langle Q \rangle$ occurs in systems consisting of a relatively small number of particles; the maximum value of N in the work of Ref. [28] is 5000 as limited by the computational time. The boundary effect may be involved. It is important to clarify if the statistical regularity in $\langle Q \rangle$ reflects the intrinsic effect of the long-range interaction or it is caused by the boundary effect.

To address this question, we shall investigate the regime of $\lambda/r_0 \ll 1$, where the boundary effect on the statistical distribution of the particles could be reduced. In terms of the number of particles, by making use of Eq. (2),

$$\frac{\lambda}{r_0} = \frac{\lambda}{a} \sqrt{\frac{2\pi}{\sqrt{3}N}} \ll 1. \quad (8)$$

Furthermore, we tune the value of λ/a to be much larger than unity for exploring the interested regime of long-range interaction. To conveniently discuss both conditions of $\lambda/r_0 \ll 1$ and $\lambda/a \gg 1$, we rewrite Eq.(8) as

$$N = \frac{2\pi}{\sqrt{3}} \left(\frac{\lambda/a}{\lambda/r_0} \right)^2 \gg 1. \quad (9)$$

Equation (9) shows that the number of particles shall be sufficiently large to simultaneously fulfill the above-mentioned two conditions. For a given value of λ/r_0 , the number of particles increases with λ/a quadratically. For the example of $\lambda/r_0 = 0.1$, when $\lambda/a = 10$, $N = 36\,275$. As the value of λ/a is increased to 20, $N = 145\,103$. By striking a balance of the limited computational resources and the required sufficiently large number of particles, in simulations we set the value of N as $N = 150\,000$, for which the disk size is as large as 10 times the screening length even when the screening length is up to 20 times the mean lattice spacing. For a shorter screening length, the ratio r_0/λ is even larger.

We first test the RBM by applying it to a relatively small system consisting of 5000 particles under varying screening length, which has been studied based on the rigorous calculations of the interacting forces [28]. It turns out that the $\langle Q \rangle$ - λ curves based on both the RBM and the rigorous calculations are almost identical as shown in Fig. 2. On both $\langle Q \rangle$ - λ curves, the sign of the time-averaged total topological charge $\langle Q \rangle$ turns from positive to negative when the value of λ is increased to about 0.3; the magnitudes of the error bars are also similar. The invariance of the $\langle Q \rangle$ - λ curve is remarkable, considering that in the calculation of the force on each particle only a few randomly picked particles instead of all of the other particles are counted. Furthermore, the histograms of the total topological charge at typical values of λ as obtained by the RBM are similar to those obtained by the rigorous calculations of the interacting forces.

Here, we shall point out that due to the approximation of the force in the RBM, the resulting microscopic particle trajectories inevitably deviate from those obtained by the rigorous calculations of the forces. However, the statistical property in question is insensitive to the discrepancy in the particle trajectories. Specifically, the agreement of the relevant results based on the RBM and the rigorous calculations shows the capability of the RBM in calculating the characteristic statistics of the topological charges in the temporally-varying particle configurations under both short- and long-range repulsions. As such, the RBM serves as a proper tool for exploring the underlying statistical regularity in the dynamical disk model. These results also suggest the robustness and effectiveness of the quantity Q for characterizing the convoluted dynamical evolutions of short- and long-range interacting particle systems.

Now, we employ the RBM to explore the large- N regime. The results are summarized in Fig. 3 for $N = 150\,000$. We collect statistically independent particle configurations in the dynamical evolution of the system in equilibrium, and we present the histograms of the total topological charge Q for $\lambda/a = 0.05$ and 20 in Figs. 3(a) and 3(b). It clearly shows that the short- and long-range interacting systems could be distinguished by the distribution of Q .

Specifically, for the case of $\lambda/a = 0.05$ in Fig. 3(a), the

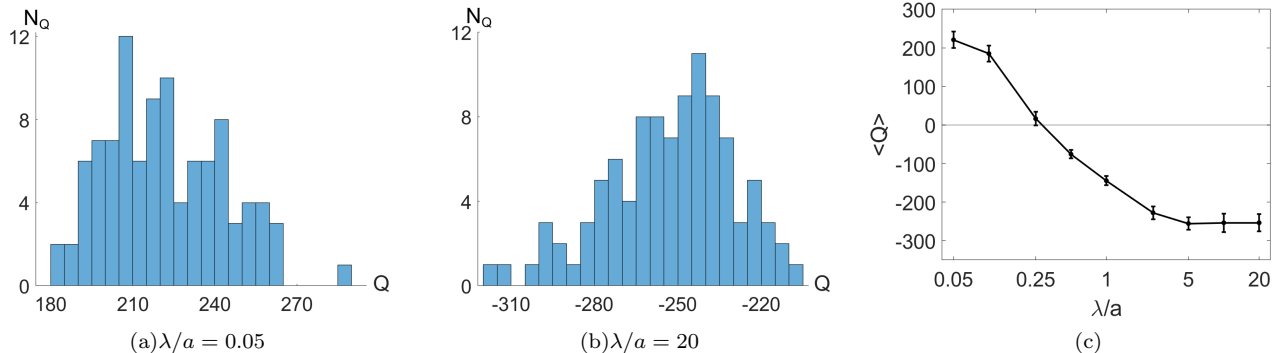


FIG. 3: Statistical regularity revealed from the perspective of total topological charge Q in the convoluted dynamical evolution of short- and long-range repulsive particles on the disk. (a) and (b) The distributions of Q in 100 statistically independent instantaneous particle configurations after the system reaches equilibrium. (c) Plot of $\langle Q \rangle$ vs the screening length λ . $\langle Q \rangle$ is the time-averaged total topological charge. The error bars indicate the magnitude of the standard deviations of Q . $N = 150\,000$.

values of Q are uniformly positive in all of the instantaneous states. In contrast, for the long-range interacting system of $\lambda/a = 20$ in Fig. 3(b), the values of Q become negative. Here, the boundary effect as measured by the ratio λ/r_0 could be ignored due to the large value of N . In both cases of $\lambda/a = 0.05$ and 20, the value of r_0 is larger than λ by at least one order of magnitude for $N = 150\,000$. Therefore, the characteristic distributions of the total topological charge Q in Fig. 3 reflect the intrinsic effect of the physical interactions on the dynamical organizations of the particles.

We further inquire how the range of the repulsive force influences the distributions of the total topological charge Q . To address this question, we systematically investigate the dynamical evolution of the particles at varying λ . The quantitative dependence of the time-averaged total topological charge $\langle Q \rangle$ on the screening length λ is shown in Fig. 3(c). We see that the $\langle Q \rangle$ -curve monotonously decreases with λ . The turning point for the value of $\langle Q \rangle$ switching from positive to negative is located at $\lambda_c \approx 0.3$.

Scrutiny of the $\langle Q \rangle$ -curves at varying N show that the value of the time-averaged total topological charge $\langle Q \rangle$ increases with the increase of N . However, the value of λ_c , where the sign of $\langle Q \rangle$ is changed, is insensitive to the variation of N . The value of λ_c is very close to 0.3 as the number of particles is increased from 5000 to 150 000. Comparison of Figs. 2 and 3 shows that the relative fluctuation of $\langle Q \rangle$ (as indicated by the relative size of the error bars) decreases with the increase of N .

B. Characteristic coarse-grained velocity field and the relaxation of particle speed

The RBM allows one to explore the large- N regime, and to perform a coarse-graining procedure for obtaining a smooth velocity field. In this subsection, from the perspective of analyzing the coarse-grained velocity field, we discuss the dynamical organizations of particles on the

disk under short- and long-range repulsive forces. Furthermore, we examine the relaxation of particle speed in large- N systems of varying λ , by which the validity of the RBM in capturing relaxation dynamics is also tested.

To obtain a smooth coarse-grained velocity field, the circumscribed square of the disk is evenly gridded into $n \times n$ square-shaped cells. Each cell is associated with a spatio-temporally averaged velocity vector, which is obtained by averaging over the velocities of the particles belonging to the specific cell and the two layers of surrounding cells for multiple instantaneous states of equal time interval δt . For revealing the characteristic behaviors of short- and long-range interacting systems, we compare the coarse-grained velocity fields under identical conditions. The values of the relevant parameters are listed here: $n = 80$, $\delta t = 2\tau_0$, and $t \in [0.1\tau_0, 60.1\tau_0]$.

In Figs. 4(a), 4(e) and 4(g), we show the coarse-grained velocity fields of distinct patterns at varying screening length; the corresponding zoomed-in plots are also presented. The color bars indicate the magnitude of kinetic energy as calculated according to the coarse-grained velocity. For the case of $\lambda = 0.05$ in Figs. 4(a)-4(d), small-scale dynamical structures are developed under the short-range repulsive force. Specifically, we identify vortices of winding number $+1$ and -1 ; the red loops and lines are introduced for visual convenience. Figure 4(b) shows a deformed $+1$ vortex surrounded by a clockwise velocity pattern. According to the elasticity theory of vortex, vortices of the same sign repel and unlike signs attract [15, 43]. Here, in the dynamical regime, we also observe a chain of connected $+1$ vortices with alternating clockwise and counter-clockwise orientations as shown in Fig. 4(c); the negative and positive signs represent clockwise and counterclockwise directions, respectively. In Fig. 4(d), we show a vortex of winding number -1 . For both $+1$ and -1 vortices, the velocity field vanishes at the central singular point in the continuum limit. As such, the regions of light color in Fig. 4(a) correspond to the singular domains of vortices. The entire velocity field

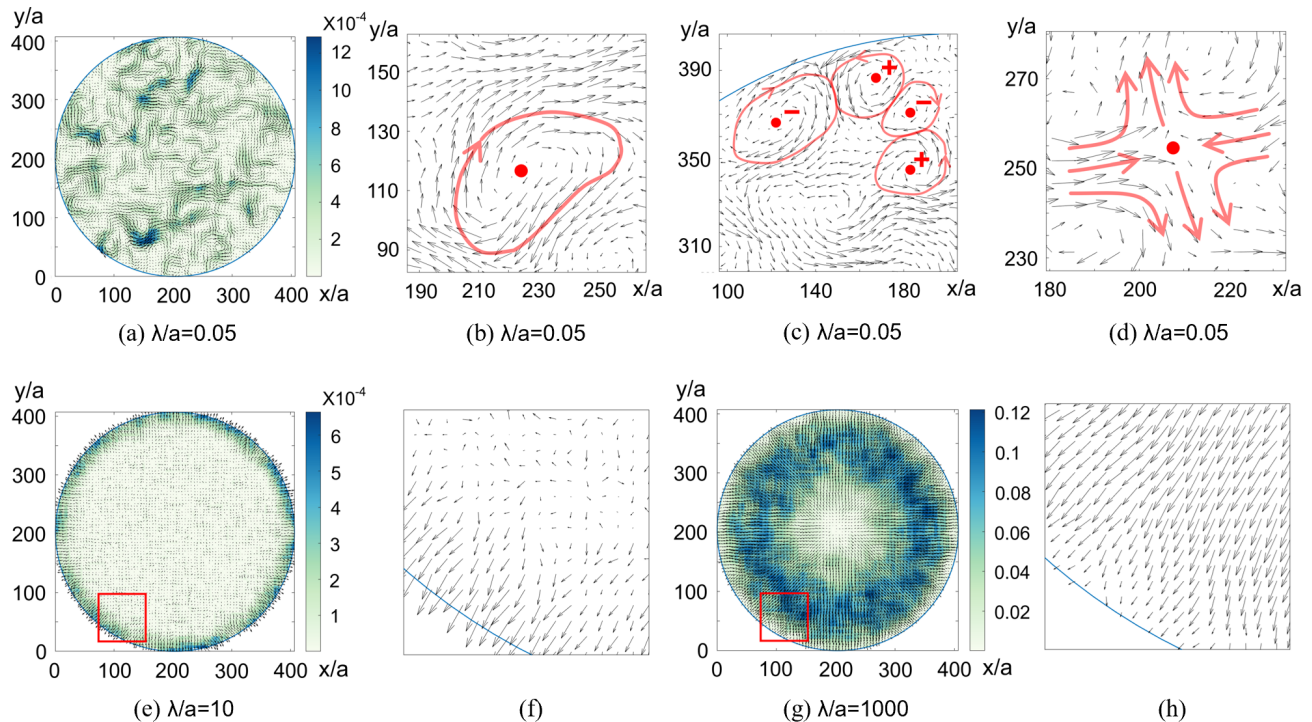


FIG. 4: Dynamical organizations of repulsive particles on the disk as demonstrated by the spatio-temporally averaged (coarse-grained) velocity field. (a), (e), and (g) are the plots of the coarse-grained velocity fields for the cases of $\lambda = 0.05$, $\lambda = 10$, and $\lambda = 1000$, respectively. The color bars besides indicate the magnitude of the kinetic energy. (b)-(d) show the local zoomed-in plots of the velocity field in (a). (f) and (h) show the local zoomed-in plots of the velocity fields in (e) and (g), respectively. The flow patterns under the short- and long-range repulsive forces are featured with the vortices of winding number ± 1 [(b)-(d)] and the outward radial flow near the boundary [(f) and (h)], respectively. The coarse-graining procedure is presented in the main text. $N = 150\,000$.

is essentially composed of vortices of winding number ± 1 .

In contrast, the coarse-grained velocity fields at early stage in systems of larger screening length are featured with the outward radial flow near the boundary, as shown in Figs. 4(e)-4(h) for the cases of $\lambda = 10$ and 1000 , respectively. The formation of the radial flow pattern could be attributed to the long-range nature of the repulsive force; the particles near the boundary are subject to outward radial force from interior particles. The boundary radial flow in the long-range repulsive systems in Figs. 4(e)-4(h) implies that the total winding number of the velocity field is $+1$. Note that this flow is connected to the phenomenon of density inhomogeneity via the accumulation of particles near the boundary in the static equilibrium packings of long-range repulsive particles on a disk [10]. Closer examination of the zoomed-in velocity fields in Figs. 4(f) and 4(h) shows that the region of the radial flow tends to extend towards the center of the disk with the increase of the screening length, indicating the enhanced alignment of velocity vectors under larger screening length. The ensuing velocity fields for both cases of $\lambda = 10$ and 1000 become highly irregular.

Comparison of the distinct velocity fields shaped by

the short- and long-range forces in Fig. 4 demonstrates the significant impact of the range of interaction on the dynamical pattern. Remarkably, the RBM is able to capture the characteristic dynamical structures in the Hamiltonian system consisting of over 100000 interacting particles. The validity of the RBM in approximating both the deterministic Hamiltonian dynamics and the stochastic dynamics has been rigorously discussed from a mathematical viewpoint [37]. Here, we provide an important physical example of a classical particle system that is of wide interest to the communities of soft matter physics and statistical physics [8, 11, 12, 28, 44].

We finally briefly discuss the relaxation process of the distribution of particle speed in both short- and long-range interacting systems by the RBM. According to the canonical ensemble formalism, the equilibrium distributions of particle position and momentum are statistically independent, if the Hamiltonian can be written as a sum of two terms containing coordinates and momenta, respectively. Thus, regardless of the range of interaction, the distribution of the particle speed is expected to converge to the Maxwell-Boltzmann distribution for the dynamical disk model consisting of a large number of par-

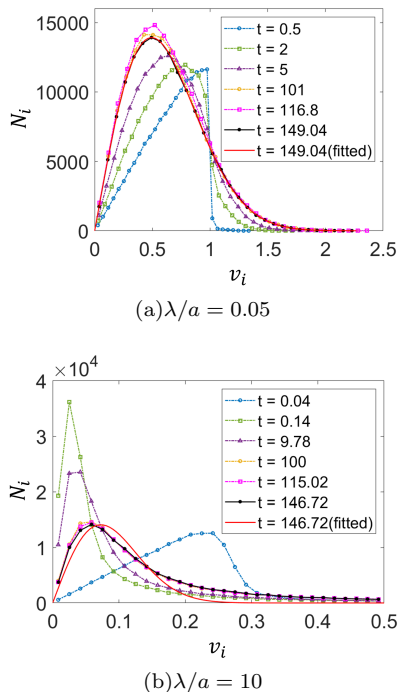


FIG. 5: The relaxation process of particle speed in short- and long-range interacting systems. The final distribution curves at $t = 149.04\tau_0$ (a) and $t = 146.72\tau_0$ (b) are fitted by the 2D Maxwell-Boltzmann distribution (solid red curves). (b) The deviation of the final distribution curve at $t = 146.72\tau_0$ (black) and its optimal fitting curve (solid red curve) could be attributed to the RBM-induced heating phenomenon. The plot range is for $v \leq 0.5$; about 10% of the fast particles whose speed exceeds 0.5 are not shown. The values of the fitting parameters: (a) $A = 615,476$, $\alpha = 2.05$, $\delta v = 0.0756$; (b) $A = 19,179,641$, $\alpha = 94.98$, $\delta v = 0.0167$. $N = 150,000$.

ticles.

The results for the cases of $\lambda/a = 0.05$ and 10 are presented in Fig. 5. We see that in both cases, the distribution curves indeed tend to converge to the 2D Maxwell-Boltzmann distribution (solid red curves):

$$f(v)\delta v = Av \exp(-\alpha v^2)\delta v, \quad (10)$$

where A and α are fitting parameters. For the case of $\lambda/a = 0.05$ in Fig. 5(a), the final distribution curve at $t = 149.04\tau_0$ (black) agrees well with the 2D Maxwell-Boltzmann distribution. For the case of $\lambda/a = 10$ in Fig. 5(b), we notice a slight deviation of the final distribution curve at $t = 146.72\tau_0$ (black) and its optimal fitting curve (red). This deviation could be attributed to the RBM-induced heating phenomenon and the procedure of cooling in simulations, which is implemented for the sake of the conservation of total energy. Note that the heating effect caused by the RBM is even more pronounced for the long-range interacting system; more information is provided in Appendix B.

From Fig. 5, we also see the distinct kinetic pathways of the relaxation process for the short- and long-range

interacting systems. For the system of $\lambda/a = 0.05$ in Fig. 5(a), the peak of the distribution curve keeps moving leftward to approach the location of the equilibrium curve. This could be understood from the perspective of energy transfer. Specifically, kinetic energy is converted into potential energy in the relaxation of the short-range interacting system (see Appendix B). In contrast, for the system of $\lambda/a = 10$ in Fig. 5(b), we observe the initial leftward and the subsequent rightward movement of the peak of the distribution curve; the rightward movement after $t \approx 2\tau_0$ corresponds to the conversion of potential energy to kinetic energy. To conclude, the relaxation process, as reflected in the movement of the peak of the speed distribution curve, is classified into two categories: the “overdamped” and the “underdamped” relaxation dynamics for the short- and long-range interacting systems, respectively. These observations imply that the short- and long-range interacting systems admit distinct microscopic dynamical modes for the relaxation of the speed distribution.

IV. CONCLUSION

In summary, we investigate the statistical and dynamical physics of the dynamical disk model consisting of a large number of repulsive particles. The recently developed powerful computational tool of the random batch method, which is specifically designed for reducing the computational complexity of long-range interacting particle systems down to the order of $O(N)$ [32, 33], allows us to explore the large- N regime of interest. To seek the order underlying the convoluted dynamical evolution of the large number of particles, we resort to the concept of a topological defect, and we reveal the intrinsic statistical regularity of topological charges that is otherwise unattainable by the continuum analysis of particle density. We further show the distinct dynamical organizations of the particles under short- and long-range repulsive forces. This work extends the disk model from the static [8–14] to the dynamical regime. We highlight the crucial role of topological defects in elucidating the intrinsic statistical order underlying the convoluted dynamical organizations of interacting particles. This work also demonstrates the promising potential of the random batch method for exploring fundamental scientific questions arising in a variety of long-range interacting particle systems in soft matter physics and other relevant fields [7, 12, 16, 17, 45].

V. ACKNOWLEDGEMENTS

This work was supported by the National Natural Science Foundation of China (Grant No. BC4190050).

Appendix A: Technical details of simulations

In this appendix, we present more information about the technical details of the boundary condition and the initial condition, and the treatment of abnormally fast particles.

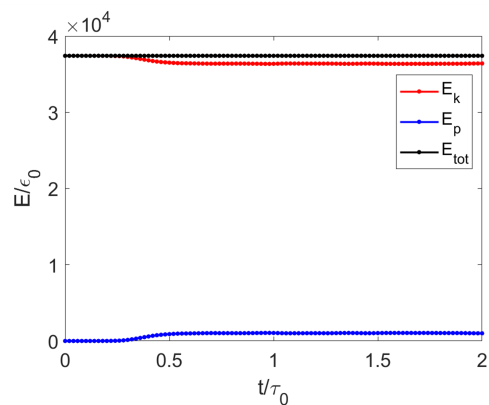
In the model, we employ the reflecting boundary to confine the point particles in the disk. For a particle that is about to collide with the boundary in a simulation step, we first identify the crossing point of the straight particle trajectory and the circular boundary, and then we let the particle make a mirror reflection with respect to the cross point. The final speed of the particle is the same as the initial incident speed prior to the reflection.

The initial state of the system is prepared by specifying a random velocity \vec{v}_{ini} and a random position \vec{r}_{ini} to each particle. The magnitude and the direction of the velocity \vec{v}_{ini} are uniform random variables. $v_{\text{ini}} \in (0, 1)$ and $\theta \in (0, 2\pi)$, where θ is the angle of the velocity vector \vec{v}_{ini} with respect to some reference direction. \vec{r}_{ini} is determined by the standard procedure of random disk packing [46]. The radius of the disk is set to be $0.3a$, where a is the mean distance of nearest particles. The values of the initial positions of the point particles in our model are given by the centers of the disks. The random disk packing prevents the aggregation of particles, which may result in a large force in a particle.

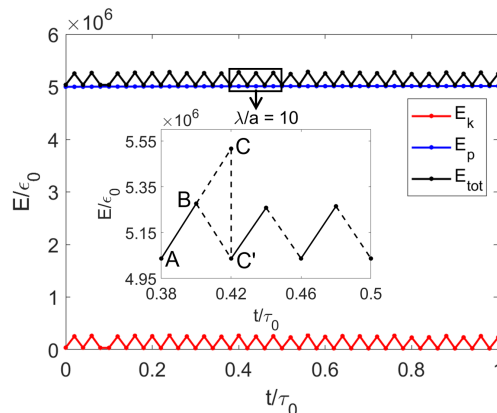
In simulations of long-range interacting systems, it is found that the speed of a small fraction of the particles (on the order of 10 in the system containing 150,000 particles) may become abnormally large; such particles cover a long distance over several a (mean distance of nearest particles) in a single simulation step. One may set the time step to be sufficiently fine to solve this problem, but such an operation is highly time consuming. In simulations, the speed of these particles is set to be zero. This operation seems to have no effect on the statistical properties of interest by a comparison with the rigorous simulations of smaller- N systems.

Appendix B: Conservation of total energy by cooling procedure

The RBM allows one to explore the large- N regime. However, it has been reported that the RBM may lead to the heating effect in molecular-dynamics simulations [33]. In our simulations, it is also found that the kinetic energy (temperature) increases monotonously in time. The heating effect could be tracked down to the partial and random selection of the particles in the calculation of the total force on a particle. Consequently, the RBM brings in temporally-varying random forces on the particles, which causes the monotonous increase of the kinetic energy (temperature). Here, we shall point out the robust statistical properties of topological charges in the presence of the thermal (random) motion of the particles caused by the RBM algorithm. A plausible explanation is



(a) $\lambda/a = 0.05$



(b) $\lambda/a = 10$

FIG. 6: The variation of kinetic and potential energies in the dynamical evolution of short- and long-range repulsive particles on the disk. The inset in (b) illustrates the cooling procedure employed in simulations for the sake of the conservation of the total energy. $N = 150\,000$.

that the magnitude of the thermal (random) motion shall exceed some critical value (comparable with the lattice spacing) to change the coordination number of a particle and thus to generate topological charge.

We employ the following cooling procedure to ensure the conservation of the total energy within some tolerance in the dynamical evolution of the system. Specifically, the energy of the system is checked periodically, and if the amount of the increased energy exceeds some threshold value (5% of the total energy $E_{\text{tot}}^{(0)}$ in the initial state), all of the velocity vectors are rescaled by a common factor $\sqrt{(E_{\text{tot}}^{(0)} - E_p)/E_k}$ to ensure that the total energy is corrected to its initial value. E_k and E_p are the kinetic energy and the potential energy at the time when the system energy is checked.

The temporally-varying energy curves in both short- and long-range interacting systems are shown in Fig. 6. For the case of $\lambda/a = 0.05$ in Fig. 6(a), the total energy is well conserved during the simulation without resorting to the cooling procedure. This could be attributed to

the rigorous calculations of the interacting forces between adjacent particles in the RBM. For the case of $\lambda/a = 10$ in Fig. 6(b), the cooling procedure is triggered when the total energy increases to be above 5% of its initial value, as indicated by the dashed vertical line from C to C' in the zoomed-in inset. Note that at the time of the checkpoint, the total energy of the system may have exceeded

5% of its initial value; for example, at the checkpoint C, the value of the total energy is about 9% of its initial value. In the data analysis, we select instantaneous states whose total energy is approximately constant; the variation of the total energy is within 5% of its initial value, as indicated by the solid black lines in Fig. 6(b).

-
- [1] Y.-J. Lai and L. I, Phys. Rev. E **60**, 4743 (1999).
- [2] J. Åström, H. Herrmann, and J. Timonen, Phys. Rev. Lett. **84**, 638 (2000).
- [3] A. Donev, F. H. Stillinger, P. Chaikin, and S. Torquato, Phys. Rev. Lett. **92**, 255506 (2004).
- [4] D. Weaire and T. Aste, *The Pursuit of Perfect Packing* (CRC, Boca Raton, FL, 2008).
- [5] A. Mughal, H. K. Chan, and D. Weaire, Phys. Rev. Lett. **106**, 115704 (2011).
- [6] V. N. Manoharan, Science **349**, 1253751 (2015).
- [7] Z. Yao, Phys. Rev. Lett. **122**, 228002 (2019).
- [8] A. Mughal and M. Moore, Phys. Rev. E **76**, 011606 (2007).
- [9] M.-C. Miguel, A. Mughal, and S. Zapperi, Phys. Rev. Lett. **106**, 245501 (2011).
- [10] Z. Yao and M. Olvera de la Cruz, Phys. Rev. Lett. **111**, 115503 (2013).
- [11] M. Cerkaski, R. G. Nazmitdinov, and A. Puente, Phys. Rev. E **91**, 032312 (2015).
- [12] V. Soni, L. R. Gómez, and W. T. Irvine, Phys. Rev. X **8**, 011039 (2018).
- [13] F. C. Silva, R. M. Menezes, L. R. Cabral, and C. C. de Souza Silva, J. Phys.: Condens. Matter **32**, 505401 (2020).
- [14] Q. Meng and G. M. Grason, Phys. Rev. E **104**, 034614 (2021).
- [15] D. R. Nelson, *Defects and Geometry in Condensed Matter Physics* (Cambridge University Press, Cambridge, 2002).
- [16] A. Bausch, M. Bowick, A. Cacciuto, A. Dinsmore, M. Hsu, D. Nelson, M. Nikolaidis, A. Travesset, and D. Weitz, Science **299**, 1716 (2003).
- [17] M. J. Bowick and L. Giomi, Adv. Phys. **58**, 449 (2009).
- [18] D. Mehta, J. Chen, D. Z. Chen, H. Kusumaatmaja, and D. J. Wales, Phys. Rev. Lett. **117**, 028301 (2016).
- [19] M. Peach and J. Koehler, Phys. Rev. **80**, 436 (1950).
- [20] J. P. Hirth and J. Lothe, *Theory of Dislocations* (Wiley, New York, 1982).
- [21] B. Halperin and D. R. Nelson, Phys. Rev. Lett. **41**, 121 (1978).
- [22] K. J. Strandburg, Rev. Mod. Phys. **60**, 161 (1988).
- [23] V. Vitelli, J. B. Lucks, and D. R. Nelson, Proc. Natl. Acad. Sci. U.S.A. **103**, 12323 (2006).
- [24] A. Azadi and G. M. Grason, Phys. Rev. Lett. **112**, 225502 (2014).
- [25] M. J. Bowick, D. R. Nelson, and H. Shin, Phys. Chem. Chem. Phys. **9**, 6304 (2007).
- [26] W. T. Irvine, M. J. Bowick, and P. M. Chaikin, Nat. Mater. **11**, 948 (2012).
- [27] Z. Yao, Soft Matter **16**, 5633 (2020).
- [28] Z. Yao, Eur. Phys. J. E **44**, 1 (2021).
- [29] H. Thomas, G. Morfill, V. Demmel, J. Goree, B. Feuerbacher, and D. Möhlmann, Phys. Rev. Lett. **73**, 652 (1994).
- [30] G. E. Morfill and A. V. Ivlev, Rev. Mod. Phys. **81**, 1353 (2009).
- [31] D. A. Walker, B. Kowalczyk, M. Olvera de la Cruz, and B. A. Grzybowski, Nanoscale **3**, 1316 (2011).
- [32] S. Jin and X. Li, Comm. Comput. Phys. **28**, 1907 (2020).
- [33] S. Jin, L. Li, and Y. Sun, Multiscale Model. Simul. **20**, 741 (2022).
- [34] J. Liang, Z. Xu, and Y. Zhao, J. Phys. Chem. A **126**, 3583 (2022).
- [35] D. Qi and J.-G. Liu, Chaos **33** (2023).
- [36] D. Frenkel and B. Smit, *Understanding molecular simulation: From algorithms to applications* (Academic Press, Cambridge, Massachusetts; 2nd edition, 2002).
- [37] S. Jin, L. Li, and J.-G. Liu, J. Comput. Phys. **400**, 108877 (2020).
- [38] F. Golse, S. Jin, and T. Paul, J. Comput. Math. **39**, 897 (2021), ISSN 0254-9409.
- [39] T. Wang, H. Chen, A. Zhou, and Y. Zhou, Comm. Comput. Phys. **30**, 1474 (2021).
- [40] J. A. Carrillo, Y. Tang, et al., Comm. Comput. Phys. **31**, 997 (2022).
- [41] J. A. Carrillo, S. Jin, L. Li, and Y. Zhu, ESAIM-Control Optim. Calc. Var. **27**, S5 (2021).
- [42] P. Chaikin and T. Lubensky, *Principles of Condensed Matter Physics* (Cambridge University Press, Cambridge, UK, 1995).
- [43] J. Sethna, *Statistical Mechanics: Entropy, Order Parameters, and Complexity* (Oxford University Press, Oxford, UK, 2006).
- [44] R. M. Menezes, E. Sardella, L. R. Cabral, and C. C. de Souza Silva, J. Phys.: Condens. Matter **31**, 175402 (2019).
- [45] A. Campa, T. Dauxois, D. Fanelli, and S. Ruffo, *Physics of Long-Range Interacting Systems* (Oxford University Press, Oxford, UK, 2014).
- [46] B. D. Lubachevsky and F. H. Stillinger, J. Stat. Phys. **60**, 561 (1990).